

Small Molecular Glasses Based on Multiposition Encapsulated Phenyl Benzimidazole Iridium(III) Complexes: Toward Efficient Solution-Processable Host-Free Electrophosphorescent Diodes

Hui Xu,* Dong-Hui Yu, Le-Le Liu, Peng-Fei Yan, Li-Wei Jia, Guang-Ming Li, and Zheng-Yu Yue*

Key Laboratory of Functional Inorganic Material Chemistry, Ministry of Education and School of Chemistry and Materials, Heilongjiang University, Harbin 150080, People's Republic of China

Received: September 28, 2009; Revised Manuscript Received: November 6, 2009

Three electrophosphorescent small molecular Ir³⁺ complexes, Ir(HexPhBI)₃ **1** (HexPhBI = 1-Hexyl-2-phenyl-1H-benzo[d]imidazole), Ir(CzPhBI)₃ **2** (CzPhBI = 9-(6-(2-phenyl-1H-benzo[d]imidazol-1-yl)hexyl)-9H-carbazole), and Ir(Cz₂PhBI)₃ **3** (Cz₂PhBI = 9-(6-(4-(1-(6-(9H-carbazol-9-yl)hexyl)-1H-benzo[d]imidazol-2-yl)phenoxy)hexyl)-9H-carbazole), were synthesized in which **3** was designed with the structure of multiposition encapsulation. Compared to the hexyl-substituted **1**, **2** and **3** end-capped with the conjugated carbazole moieties have improved thermal stability. X-ray diffraction analysis proved the amorphous state of **2** and **3**. High-photoluminescent efficiencies of **3** are achieved as 72% in solution and 61% in solid. It indicates that the peripheral carbazoles not only facilitate the separation of triplet-emission cores and reduce the intermolecular aggregation but also supply a routine for the intermolecular energy transfer. Electrochemical analysis showed the more oxidation states of **3**, which might be anticipated to make it superior to **1** and **2** in hole injection and transporting. The important role of the peripheral carbazole moieties in carrier injection/transporting and the optical properties of the complexes were further investigated by Gaussian simulation. A dramatic electroluminescent (EL) performance, including external quantum efficiency of nearly 6%, low turn-on voltage of 2.5 V, and high brightness over 6000 cd m⁻², from the host-free spin-coated device of **3** was achieved. The superiority of multiencapsulation in EL was proved by comparing the EL performance of **2** and **3**. By making comparison between the host-free and phosphor-doping devices, it indicated that the combined modification of the aliphatic chains and functional groups in multipositions is a feasible approach to realize the high-efficiency small molecular phosphorescent materials.

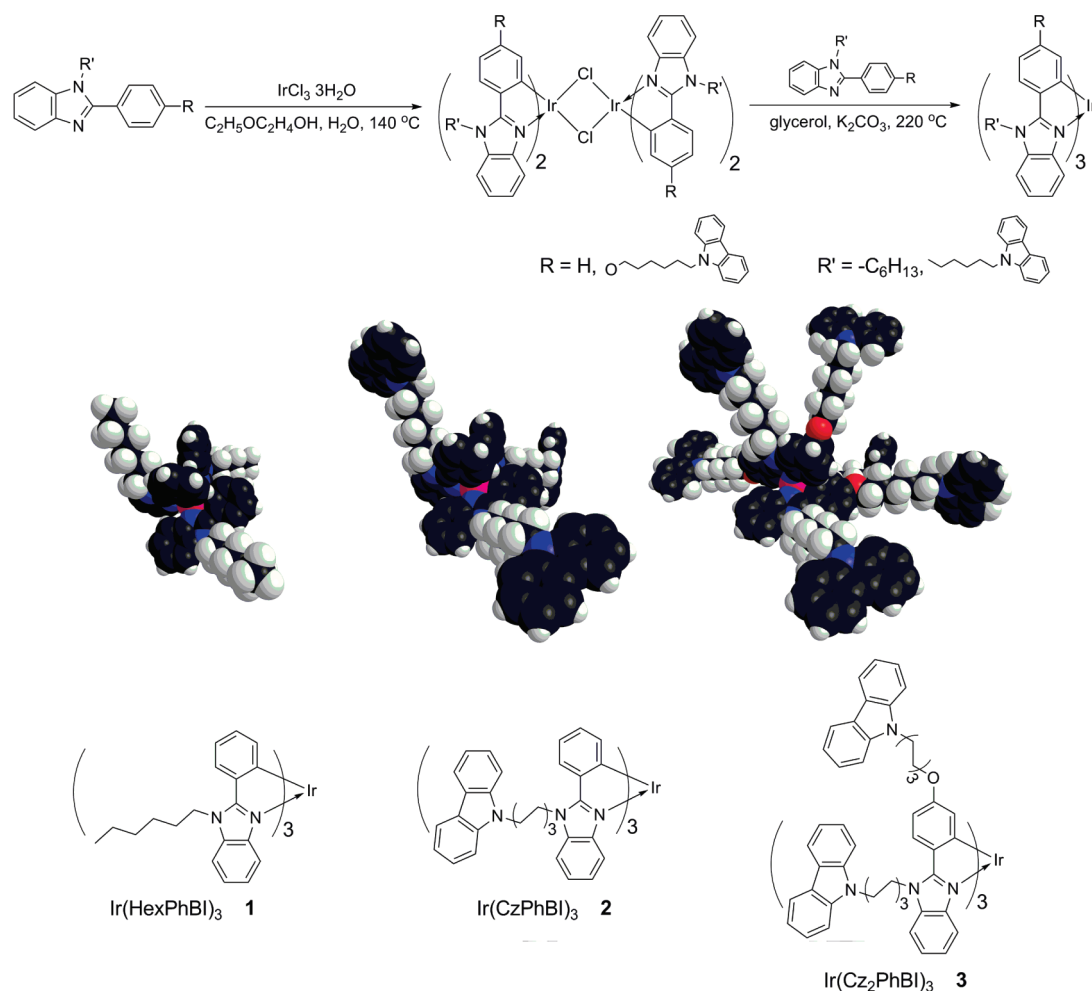
Introduction

The organic light-emitting diodes (OLEDs) based on the electrophosphorescent emitters have been paid much attention with the great potential for full-color flat-panel displays and light sources.^{1,2} Since the phosphorescent emitters can harvest both singlet and triplet excitons, their theoretical internal electroluminescent (EL) quantum efficiency can reach 100%.¹ However, most of the phosphorescent emitters present the worse concentration quenching and triplet–triplet (T-T) annihilation in their solid states.³ The external quantum efficiency (EQE) of the devices using pure Ir(ppy)₃ (ppy = 2-phenylpyridine) as the emitting layers was less than 0.8%.² To reduce the concentration quenching, the common approach is doping/blending^{3,4} the emitters in suitable host systems. Hosts, such as polyvinylcarbazole (PVK), 2-(biphenyl-4-yl)-5-(4-*tert*-butylphenyl)-1,3,4-oxadiazole (PBD), and poly(9,9-dioctylfluorene) (PFO), served as the energy media and the matrixes dispersing the phosphorescent emitters. Many excellent performances were realized.^{4–17} However, these doping/blending systems were inferior in phase stability, processability, and repeatability. One of the main solutions is linking the hosts and guests through covalent bonds. The electrophosphorescent dendrimers and polymers were designed as the integrations of hosts and guests for the host-

free or heavy-blending devices.^{15–27} Because of their controllable intermolecular interactions and reduced T-T quenching, they are expected as the alternatives to the doping/blending systems. Actually, dendrimers and polymers also have another important advantage of solution processability. Although the solution-processed electrophosphorescent devices exhibited worse performances than the corresponding vacuum-deposited devices, it is believed that the approaches of solution-process are much more desirable for low-cost large-area commercial applications.¹⁰ The devices based on these pure dendrimers, as well as phosphorescent polymers, exhibited good EL performance. Also recently with the introduction of several functional dendrons based on carbazole, triphenyl amine, fluorene moieties, and the design of “double-dendron” configuration, the electrophosphorescent performance of the dendrimers has been improved greatly.^{22,28,30} Relatively, the polymer and dendrimer systems are complicated and have some difficulties in synthesis. How to benefit from the structure design of the dendrimers and achieve an excellent EL performance through simpler molecular structures is an interesting and significant challenge.

Recently, the small molecular electrophosphorescent emitters with reduced concentration quenching for the host-free OLEDs became attractive. Several nondoped vacuum-deposition devices of pure small molecules with high efficiencies were reported;^{6,31–35} however, there are still few reports about the similar host-free devices through solution-process. Efficient small molecular solution-processable amorphous phosphors would be superior

* To whom correspondence should be addressed. Tel: +86 451 81773032. Fax: +86 451 86608042. E-mail: (H.X.) hxu@hlju.edu.cn and (Z.-Y.Y.) yuezhengyu@hlju.edu.cn.

SCHEME 1: Synthesis Procedure and the Molecular Structures of the Ir³⁺ Complexes

in synthesis, processability, and stability and have the potential as one of the most important alternative for host-free solution-processed electrophosphorescent devices. It is well-known that the separation of triplet excitons can efficiently decrease the quenching effect.^{2,29} For small molecules, the flexible aliphatic chains cannot only efficiently restrain the intermolecular interaction and aggregation but also improve the dissolvability and film-forming ability. However, according to the previous works about dendrimers, only using aliphatic moieties as the wrapping groups the electric performance of the materials would remarkably decrease. Recently, we reported a series of zinc(II) complexes based on carbazol-9-yl hexyl modified (hydroxyl-phenyl) benzimidazole.³⁶ This rigid ring end-capped aliphatic chain can remarkably decrease the aggregation, which induced the hypsochromic emission of the complex. The peripheral carbazole moieties also played an important role in the carrier injection/transporting. However, for phosphorescent molecules, only one position modification is not enough. Thanks to the pioneer work reported by Burn et al.,²⁵ multiposition encapsulation seems to be essential for our molecular design.

In this work, a double-position modified phenyl benzimidazole ligand 9-(6-(4-(1-(6-(9H-carbazol-9-yl)hexyl)-1H-benzo[d]imidazol-2-yl)phenoxy)hexyl)-9H-carbazole (Cz₂PhBI) and its six-position encapsulated complex Ir(Cz₂PhBI)₃ **3** were designed and conveniently synthesized, as well as Ir(HexPhBI)₃ **1** (HexPhBI = 1-Hexyl-2-phenyl-1H-benzo[d]imidazole) and Ir(CzPhBI)₃ **2** (CzPhBI = 9-(6-(2-phenyl-1H-benzo[d]imidazol-1-yl)hexyl)-9H-carbazole) for comparison (Scheme 1). The

peripheral carbazole moieties were introduced to inject/transport hole and sensitize the Ir³⁺ complex cores. The flexible hexyls can reduce the intermolecular interaction and facilitate the solution-process of the complexes. Gaussian simulation indicated that the electron-cloud densities of the frontier orbitals (the highest occupied molecular orbital (HOMO), HOMO-1, HOMO-2, the lowest unoccupied molecular orbital (LUMO), LUMO+1 and LUMO+2) of the complexes were entirely located on the cores formed by Ir³⁺ and phenyl benzimidazole moieties. Therefore, the flexible hexyls and carbazole moieties surrounding the cores actually form the peripheral shell to isolate the excitons. According to the space-filling models, the double bulky chains of **3** point to six different directions and almost fill in all of the blank spaces in **2** (Scheme 1). The investigation showed that the carbazole end-capped aliphatic chains facilitate the formation of amorphous state of the complex more efficiently. Moreover, **3** with a very high PL quantum yield (PL QY) of more than 60% in film exhibits much weaker quenching effect than **1** and **2**. Considering the strong wrapping effect of the aliphatic chains, the biggest degree of encapsulation of the core in **3** will make a remarkable contribution to its lower exciton concentration and weaker intermolecular interaction. Both electrochemical results and Gaussian simulation indicated the important role of the peripheral carbazole moieties as the intermolecular hole-transfer groups. The EL performance of the host-free spin-coated OLED based on **3** was improved as much as twice of that of **2**.

Experimental Section

Materials and Instruments. All the reagents and solvents used for the synthesis of the ligands and complexes were purchased from Aldrich and Acros companies and used without further purification.

Infrared spectra were recorded using a Bruker-EQUINOX55 FT-IR spectrometer. ^1H NMR spectra were recorded using a Varian Mercury plus 300NB spectrometer relative to tetramethylsilane (TMS) as internal standard. Molecular masses were determined by a FINNIGAN LCQ Electro-Spraying Ionization-Mass Spectrometry (ESI-MS), or a MALDI-TOF-MS. Elemental analyses were performed on a Vario EL III elemental analyzer. Absorption and photoluminescence (PL) emission spectra of the target compound were measured using a SHIMADZU UV-3150 spectrophotometer and a SHIMADZU RF-5301PC spectrophotometer, respectively. Thermogravimetric analysis (TGA) and differential scanning calorimetry (DSC) were performed on Shimadzu DSC-60A and DTG-60A thermal analyzers under nitrogen atmosphere at a heating rate of $10\text{ }^\circ\text{C min}^{-1}$. Cyclic voltammetry (CV) was performed on an Eco Chemie's Autolab.

2-Phenyl-benzimidazole. Benzene-1,2-diamine (27.0 g, 0.25 mol) and benzaldehyde (25.28 mL, 0.25 mol) were solved in 200 mL DMF. Then sodium metabisulfite (47.53 g, 0.25 mol) in 50 mL water was added in portions. The mixture was heated to $90\text{ }^\circ\text{C}$ overnight and then cooled to room temperature and poured into water. The precipitate was filtered and then recrystallized by ethanol as white needle crystals (42.0 g, 82%). mp $295\text{--}296\text{ }^\circ\text{C}$. ^1H NMR (300 MHz, DMSO- d_6 , TMS): $\delta = 12.92$ (s, N-H, 1H); 8.21 (d, $J = 6.9$ Hz, 2H); 7.77–7.43 (m, 5H); 7.23 ppm (d, $J = 4.8$ Hz, 2H). ESI-MS m/z (%): 194 (100) [M^+]. Elemental anal calcd (%) for $\text{C}_{13}\text{H}_{10}\text{N}_2$: C, 80.39; H, 5.19; N, 14.42. Found: C, 80.43; H, 5.28; N, 14.29.

4-(1H-Benzimidazol-2-yl)phenol. The synthetic procedure was the same as 2-phenyl-benzimidazole, but 4-hydroxybenzaldehyde was used instead of benzaldehyde (45.0 g, 85%). mp $281\text{--}282\text{ }^\circ\text{C}$. ^1H NMR (300 MHz, DMSO- d_6 , TMS): $\delta = 12.64$ (s, N-H, 1H); 9.96 (s, O-H, 1H); 8.03 (d, $J = 8.7$ Hz, 2H); 7.73–7.36 (m, 2H); 7.25–7.09 (m, 2H); 6.94 ppm (d, $J = 8.4$ Hz, 2H). ESI-MS m/z (%): 210 (100) [M^+]. Elemental anal calcd (%) for $\text{C}_{13}\text{H}_{10}\text{N}_2\text{O}$: C, 74.27; H, 4.79; N, 13.33; O, 7.61. Found: C, 74.38; H, 4.81; N, 13.54; O, 7.27.

General Procedure for Preparation of the Ligands. Under N_2 , the benzimidazole derivatives were dissolved in acetone. The equivalent KOH was added and the mixture was stirred for 30 min. Then the bromides were added in portions. The mixture was heated to reflux for overnight and quenched by water, and then the mixture was extracted by dichloromethane (3×30 mL). The organic layer was dried with MgSO_4 . The solvent was removed in vacuo. The residues were recrystallized with petroleum ether/ethyl acetate (1:1).

1-Hexyl-2-phenyl-1H-benzimidazole (HexPhBI). White crystals with yield of 55%. mp $40\text{--}42\text{ }^\circ\text{C}$. ^1H NMR (300 MHz, CDCl_3 , TMS): $\delta = 7.87\text{--}7.79$ (m, 1H); 7.28 (dd, $J_1 = 7.8$ Hz, $J_2 = 5.4$ Hz, 2H); 7.57–7.48 (m, 3H); 7.46–7.37 (m, 1H); 7.35–7.27 (m, 2H); 4.25 (t, $J = 7.5$ Hz, 2H); 1.89–1.73 (m, 2H); 1.29–1.15 (m, 6H); 0.85 ppm (t, $J = 6.9$ Hz, 3H); ESI-MS m/z (%): 278 (100) [M^+]. Elemental anal calcd (%) for $\text{C}_{19}\text{H}_{22}\text{N}_2$: C, 81.97; H, 7.97; N, 10.06. Found: C, 81.78; H, 7.89; N, 10.33.

9-(6-(2-Phenyl-1H-benzimidazol-1-yl)hexyl)-9H-carbazole (CzPhBI). White crystals with yield of 90%. mp $114\text{--}116\text{ }^\circ\text{C}$. ^1H NMR (300 MHz, CDCl_3 , TMS): $\delta = 8.10$ (d, $J = 7.8$ Hz, 2H); 7.879–7.768 (m, 1H); 7.72–7.62 (m, 2H); 7.51–7.39 (m, 5H); 7.36–7.28 (m, 5H); 7.25 (t, $J = 7.8$ Hz, 2H); 4.24 (tt,

$J_1 = 6.9$ Hz, $J_2 = 7.5$ Hz, 2H); 1.84–1.65 (m, 4H); 1.36–1.12 (m, 4H); ESI-MS m/z (%): 443 (100) [M^+]. Elemental anal calcd (%) for $\text{C}_{31}\text{H}_{29}\text{N}_3$: C, 83.94; H, 6.59; N, 9.47. Found: C, 83.85; H, 6.57; N, 9.58.

9-(6-(4-(1-(6-(9H-Carbazol-9-yl)hexyl)-1H-benzimidazol-2-yl)phenoxy)hexyl)-9H-carbazole (Cz₂PhBI). White crystals with yield of 78%. mp $128\text{--}132\text{ }^\circ\text{C}$. ^1H NMR (300 MHz, CDCl_3 , TMS): $\delta = 8.11$ (dd, $J_1 = 7.5$, $J_2 = 6.9$ Hz, 4H); 7.82–7.76 (m, 1H); 7.59 (d, $J = 8.7$ Hz, 2H); 7.50–7.36 (m, 6H); 7.36–7.17 (m, 9H); 6.96 (d, $J = 8.7$ Hz, 2H); 4.33 (t, $J = 7.2$ Hz, 2H); 4.23 (t, $J = 6.9$ Hz, 2H); 4.17 (t, $J = 7.5$ Hz, 2H); 3.96 (t, $J = 6.6$ Hz, 2H); 1.99–1.85 (m, 2H); 1.84–1.58 (m, 8H); 1.30–1.18 (m, 6H). ESI-MS m/z (%): 708 (100) [M^+]. Elemental anal calcd (%) for $\text{C}_{49}\text{H}_{48}\text{N}_4\text{O}$: C, 83.02; H, 6.82; N, 7.90; O, 2.26. Found: C, 83.14; H, 6.79; N, 8.08; O, 2.11.

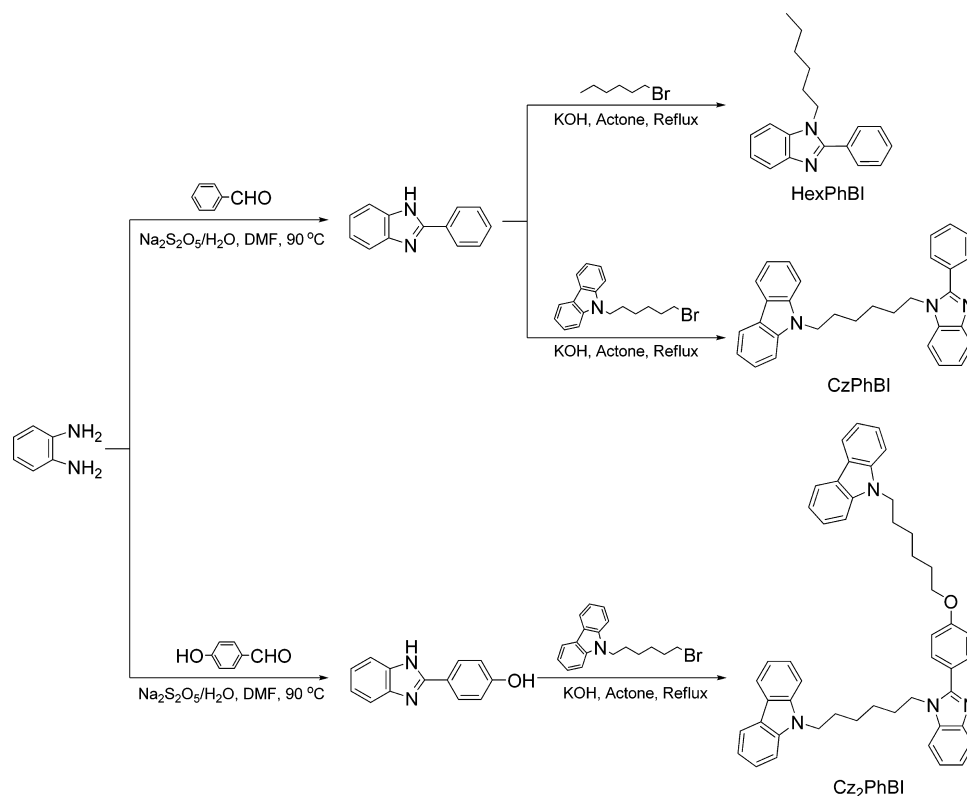
General Procedure for Preparation of Ir³⁺ Complexes. Under N_2 , iridium trichloride hydrate (1 mmol, 267 mg) was added to a solution of the ligands (1 mmol) in 2-methoxyethanol (30 mL) and water (10 mL). The mixture was heated to $120\text{ }^\circ\text{C}$ with constant stirring for one day and then cooled to room temperature. The amorphous green precipitates were filtrated, washed with water (3×30 mL) and methanol (3×30 mL), dried and used as the crude dichloro-bridged iridium dimers. The mixture of the dimers (0.2 mmol), the corresponding ligands (0.44 mmol), and anhydrous K_2CO_3 (67 mg, 0.50 mmol) in glycerol (10 mL) was heated to $210\text{ }^\circ\text{C}$ for 2 days and then cooled to room temperature. Excess water was added. The solution was extracted with CH_2Cl_2 (3×30 mL). The organic phase was dried with MgSO_4 . The solvent was removed in vacuo. The residues were purified by the flash column chromatography using CH_2Cl_2 as eluent to afford the complexes.

Ir(HexPhBI)₃ 1. Orange powder with yield of 25%. ^1H NMR (300 MHz, CDCl_3 , δ): 7.74 (t, $J = 7.8$ Hz, 3H), 7.267–6.43 (m, 15H), 6.28 (t, $J = 7.8$ Hz, 3H), 6.13 (d, $J = 8.4$ Hz, 3H), 4.63 (tt, $J_1 = 7.2$ Hz, $J_2 = 7.2$ Hz, 6H), 2.06–1.78 (m, 6H), 1.41–1.12 (m, 18H), 0.91 ppm (t, $J = 6.9$ Hz, 9H). MALDI-TOF-MS (m/z (%)): 1026 (100) [M^+]. Anal. Calcd (%) for $\text{C}_{57}\text{H}_{65}\text{IrN}_6$: C, 66.70; H, 6.38; N, 8.19. Found: C, 66.77; H, 6.46; N, 8.02.

Ir(CzPhBI)₃ 2. Yellow powder with yield of 35%. ^1H NMR (300 MHz, CDCl_3 , δ): 8.09 (d, $J = 7.8$ Hz, 6H), 7.58 (d, $J = 7.2$ Hz, 3H), 7.44 (t, $J = 7.8$ Hz, 6H), 7.28 (d, $J = 9.0$ Hz, 6H), 7.23 (t, $J = 7.5$ Hz, 6H), 7.14 (d, $J = 8.1$ Hz, 3H), 6.85–6.69 (m, 6H), 6.58 (t, $J = 7.5$ Hz, 3H), 6.07 (d, $J = 8.1$ Hz, 3H), 4.65–4.31 (m, 6H), 4.23–4.04 (m, 6H), 1.95–1.68 (m, 12H), 1.42–1.23 ppm (m, 12H). MALDI-TOF-MS (m/z (%)): 1521 (100) [M^+]. Anal. Calcd (%) for $\text{C}_{93}\text{H}_{86}\text{IrN}_9$: C, 73.39; H, 5.70; N, 8.28. Found: C, 73.41; H, 5.77; N, 8.15.

Ir(Cz₂PhBI)₃ 3. Green-yellow powder with yield of 32%. ^1H NMR (300 MHz, CDCl_3 , δ): 8.07 (d, $J_1 = 7.8$ Hz, $J_2 = 2.4$ Hz, 12H), 7.47–7.29 (m, 24H), 7.25–7.13 (m, 18H), 7.07 (d, $J = 8.1$ Hz, 3H), 6.87–6.74 (br, 3H), 6.54 (t, $J = 7.5$ Hz, 3H), 6.25–6.08 (br, 3H), 6.00–5.84 (br, 3H), 4.47–3.93 (m, 24H), 1.81–1.61 (m, 18H), 1.35–1.14 (m, 30H). MALDI-TOF-MS (m/z (%)): 2318 (100) [M^+]. Anal. Calcd (%) for $\text{C}_{147}\text{H}_{143}\text{IrN}_{12}\text{O}_3$: C, 76.17; H, 6.22; N, 7.25; O, 2.07. Found: C, 76.31; H, 6.19; N, 7.38; O, 2.36.

Theoretical Calculations. Computations on the electronic ground state of the ligands and complexes were performed using Becke's three-parameter density functional in combination with the nonlocal correlation functional of Lee, Yang, and Parr (B3LYP).³⁷ 6-31G(d) basis sets were employed for the ligand and the relativistic effective core potential of Los Alamos and double- ζ basis sets were employed for the Ir (LANL2DZ).³⁸

SCHEME 2: Synthesis Procedure of the Ligands

The ground-state geometries were fully optimized at the B3LYP level. All computations were performed using the Gaussian 03 package.³⁹

Device Fabrication and Testing. The OLEDs with configurations of ITO/PEDOT:PSS (50 nm)/Ir³⁺ complexes (30 nm)/TPBI(30 nm)/LiF (1 nm)/Al (100 nm) and ITO/PEDOT:PSS (50 nm)/Ir³⁺ complexes–TCTA (20%, 30 nm)/TPBI (30 nm)/LiF (1 nm)/Al (100 nm), where PEDOT:PSS is poly(3,4-ethylenedioxythiophene):poly(styrene sulfonate) as hole-injection/transporting layer, TPBI is 1,3,5-tris(1-phenyl-1H-benzimidazol-2-yl)benzene as electron-transporting hole-blocking layer, and TCTA is tris(4-(9H-carbazol-9-yl)phenyl)amine as host, were fabricated as in the following procedure: PEDOT:PSS films were first deposited on precleaned ITO-coated glass substrates and then cured at 120 °C in air for 30 min. Then the film of the emitting layer was spin-cast with chlorobenzene as the solvent (concentration: 10 mg mL⁻¹) at a spin rate of 1200 rpm, followed by deposition of TPBI at a rate of 0.2 nm s⁻¹ at a pressure below 1 × 10⁻⁶ mbar. Then a layer of LiF with 1 nm thickness was deposited at a rate of 0.1 nm s⁻¹ to improve electron injection. Finally, a 100 nm thick layer of Al was deposited at a rate of 0.6 nm s⁻¹ as the cathode. The EL spectra were measured using a PR650 spectra colorimeter. The current–density–voltage and brightness–voltage curves of the devices were measured using a Keithley 2400/2000 source meter and a calibrated silicon photodiode. All the experiments and measurements were carried out at room temperature under ambient conditions.

Results and Discussions

Design and Synthesis. To reduce the T-T quenching, one of the most efficient approaches is separating the phosphorescent centers. Although some simple aryl groups can be used to encapsulate the complex cores, their strong π - π stacking

interaction would increase the intermolecular interaction. Thus, if using aryl groups it is necessary to restrain the intermolecular interaction through the steric effect by increasing the volume of the aromatic substituents or the angle of torsion between them. Many electrophosphorescent dendrimers had the similar multiaryl substituted structures. With the aim of achieving a simple small molecular phosphor used in host-free spin-coated devices, alkyl moieties are more suitable as the encapsulating groups, which not only reduce the intermolecular interaction efficiently by steric effect and easily wrap the complex cores to separate the phosphors, but also improve the solution-processability of the complex. However, along with the reduction of interaction between the complex cores, the electric inertia of the alkyls also remarkably weakens the carrier injection/transporting in the materials. Recently, it was reported by Samuel et al.⁴¹ that although their Ir³⁺ cores were also separated, carbazole dendrons made a great contribution to the improvement of the carrier injection/transport in the dendrimers. Therefore, we believed that the combinations of carrier-transporting moieties and aliphatic chains (CT-AC), such as the carbazole end-capped alkyls in this work, should be the suitable encapsulating groups for the small molecular electrophosphorescent complexes. The CN ligands we chose were 2-phenyl-benzimidazole (PBI) derivatives. The N–H in benzimidazole rings supplied one position for alkyl substitution. Through introducing a hydroxyl at para-position of phenyl, a double-position substitutable PBI derivative was obtained. The space-filling models simulated by Gaussian calculation showed that after alkylation six bulky arms were formed in **3**, which point to six different directions and almost fill in all of the blank spaces in three carbazole-9-yl hexyl encapsulated **2** (Scheme 1). This strongly demonstrated our molecular design.

The PBI derivatives were synthesized by condensation of benzaldehyde derivatives and *o*-phenylenediamine with the

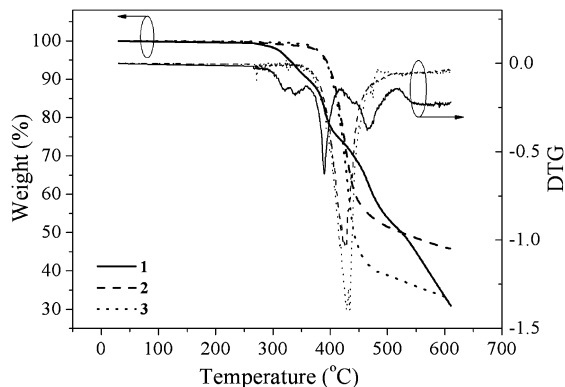


Figure 1. TGA and DTG curves of 1–3.

existence of a mild oxidant sodium metabisulfite. Then the ligands were prepared conveniently by alkylation of the PBI derivatives with different alkyl bromides under alkaline conditions as depicted in Scheme 2. The Ir³⁺ complexes were prepared according to the following well-established, two-step approach⁴⁰ (Scheme 1): the chloride-bridged dimers were first formed by treating IrCl₃·nH₂O with excessive ligands in a mixed solvent of 2-ethoxyethanol and water. Then the crude dimers reacted with excessive ligands to convert to the facial (fac) isomer at 210 °C in glycerol. The complexes were purified through flash column chromatography and characterized by ¹H NMR, elemental analysis, and MALDI-TOF mass spectrometry.

Thermal and Phase Properties. The temperatures of decomposition (*T_d*) of **1** is 330 °C. *T_d* of **2** and **3** increases to 402 °C (Figure 1). It was found that **1** started decomposition at 273 °C, and at 398 °C the weight loss ratio was 24%, which just corresponds to the loss of three hexyls in **1**. However, for **2** and **3** the decomposition occurred from 360 °C. At 490 °C, the weight loss ratios of **2** and **3** were 48 and 61%, respectively, which are attributed to the loss of the carbazol-9-yl hexyls in **2** and **3**. It means that the decomposition of the hexyls at lower temperature can be efficiently prevented by end-capping with carbazole moieties. The intra- and intermolecular π – π interactions between different carbazole moieties may retard the decomposition of hexyls, since the additional interactions make the decomposition need more energy, which might be the main reason for the improved thermal stability of **2** and **3**.

The phase states of the complexes are what we were very concerned about, because the amorphous or disordered states often correspond to the weak intermolecular interaction, which is very important for decreasing T-T quenching. Although the complexes did not have any melting points according to their DSC analysis, in order to clearly find out the phase status of the spin-coated films, wide-angle X-ray diffraction (WAXRD) analysis of **1**–**3** was performed (Figure 2). For **1** two sharp peaks with 2θ angles at 8 and 20° proved the existence of crystallization in **1**. Obviously, only with the alkyl substitution the aggregation of the Ir³⁺ cores cannot be avoided absolutely. Although it was doubt if the planar structure of carbazole might facilitate aggregation, only the broad and weak peaks were found in the WAXRD spectra of **2** and **3**. Moreover, the broad peak around 8° in the spectrum of **3** was much weaker than that of **2** and hardly to be recognized. Both **2** and **3** are amorphous. It means that the bulky carbazol-9-yl hexyl moieties in **2** and **3** efficiently prevent the aggregation, and **3** with more carbazol-9-yl hexyls seems to be more disordered. It is clear that the intermolecular interaction and aggregation of **3** is the weakest among these three complexes, which might have strong effects on the reduction of concentration quenching and T-T annihilation.

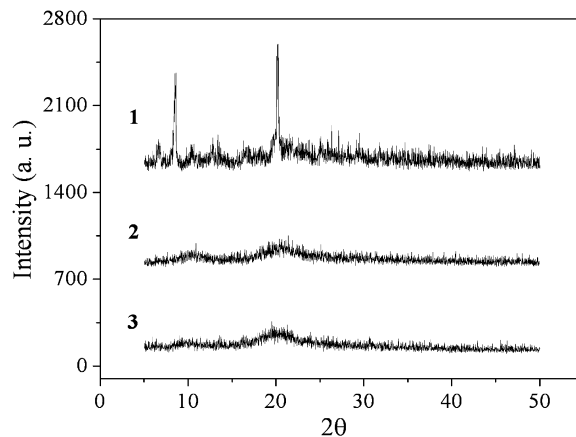


Figure 2. WAXRD spectra of 1–3.

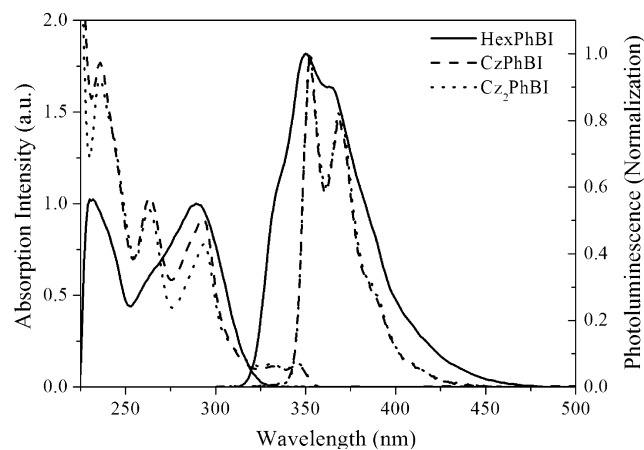


Figure 3. The absorption and PL spectra of the ligands in solution.

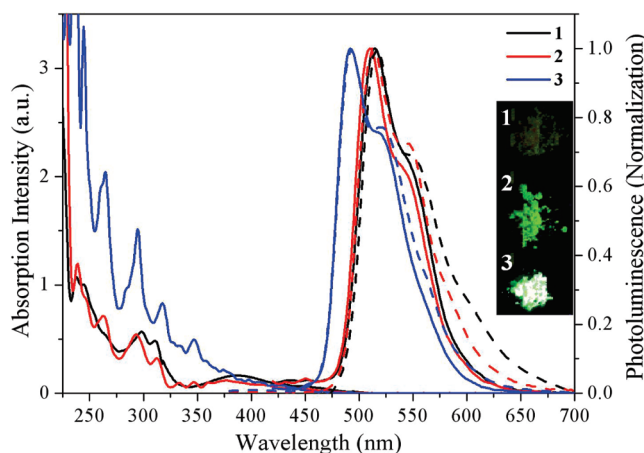


Figure 4. The absorption and PL spectra of 1–3 in solution (solid) and film (dash) and the emission photos of the complexes (insert, for **3** because CCD camera was saturated the emission looks like white.)

Optical Properties. To examine the photophysical properties of the complexes, UV/vis and PL spectra of the ligands and **1**–**3** were measured in their dilute CH₂Cl₂ solutions (1×10^{-5} mol L⁻¹) (Figures 3 and 4). The absorption peak at 289 nm of HexPhBI is attributed to the benzimidazole moieties, and the other peak at 231 nm corresponds to its phenyl moiety. For CzPhBI and Cz₂PhBI, except for the absorption peaks originated from phenyl benzimidazole, the peaks at 346, 332, 263, and 236 nm are attributed to their carbazole moieties. Notably, the emissions of CzPhBI and Cz₂PhBI are similar to that of

TABLE 1: The PL and Electrochemical Properties of the Compounds

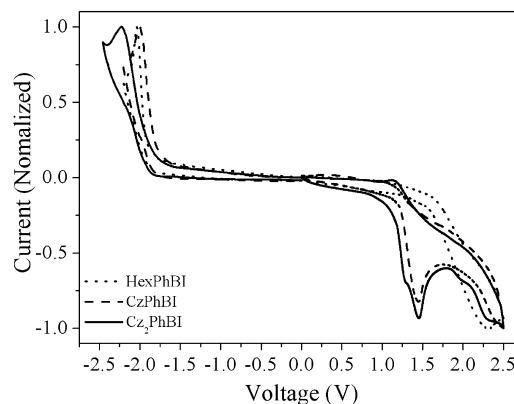
compound	absorption peaks (nm) ^a	PL peaks (nm) ^a	PL QY	τ_{PH} (μs)	$E_{\text{ox}}/E_{\text{red}}$ (V) ^d	HOMO (eV)	LUMO (eV)	E_g (eV)
HexPhBI	289, 231	350, 365(s)			1.65/−1.78	−6.39	−2.96	3.43
CzPhBI	346, 332, 293, 263, 236, 221	352, 368			1.18/−1.73	−5.92	−3.01	2.91
Cz ₂ PhBI	346, 332, 293, 263, 236, 221	352, 368			1.00/−1.81	−5.74	−2.93	2.81
1	445, 423, 388, 311, 298, 245, 227	514, 546(s)	0.20 ^b /0.11 ^c	0.39	0.44/−1.74	−5.18	−3.0	2.18
2	445, 413, 376, 346, 312, 294, 262, 239	509, 541(s)	0.34 ^b /0.20 ^c	0.34	0.43/−1.77	−5.17	−2.97	2.20
3	428, 407, 373, 349, 317, 295, 267, 237	491, 517(s)	0.72 ^b /0.61 ^c	0.20	0.39/−1.84	−5.13	−2.9	2.23

^a 10^{-6} M in CH_2Cl_2 . ^b 10^{-6} M in degassed toluene using quinine sulfate in 0.5 M sulfuric acid as standard. ^c PL QY of the spin-coated films. ^d Onset voltages in CV curves.

N-substituted carbazole derivatives, which proves the antenna effect of the carbazole moieties in these alkyl linked donor–acceptor systems.

Compared with the absorption spectra of the ligands, in the absorption spectra of **1–3**, the strong absorption bands observed at 230–350 nm closely resemble those of the free ligands. Especially for **2** and **3** the absorption peaks originated from the carbazole moieties around 346 and 262 nm are recognized and become stronger along with the increasing of the density of carbazoles. These short-wavelength absorptions are assigned to a ligand-centered $^1\pi-\pi^*$ transition. The broad absorption peaks around 400 nm are metal-to-ligand charge-transfer (MLCT) transitions. The next long tail absorptions from 450 to 500 nm can reasonably be assigned to the mixed states containing spin–orbit coupling enhanced $^3\pi-\pi^*$ and $^3\text{MLCT}$ transitions.

PL emission of **1** contains a main peak at 514 nm. The emission of **2** is at 509 nm with a slight blue shift of 5 nm, which should be induced by the influence of pendent carbazoles on the energy of MLCT state through changing the coordinate environment, local polarity and polarizability of the complex. A much more remarkable hypsochromic shift of the emission of **3** was observed as 20 nm (the main peak of **3** is at 491 nm). With the exception that more pendent carbazoles induced stronger changing of the energy of MLCT state, the effect of the electron-donating alkoxy moieties on the frontier orbitals of **3** should be the main factor for this considerable blue shift. It is also noticeable that the PL spectrum of **3** in solution displays much more discernible vibronic progressions than those of **1** and **2**; in addition, in films from **1**, **2**, to **3** the intensity of their shoulder peaks gradually increase. These features suggest the successively increased molecular rigidity from **1**, **2**, to **3**. Furthermore, the emissions of these complexes in solutions and spin-coated films are nearly the same, which also showed their reduced aggregation in solid. PL QY of the complexes in solution gradually increases from **1**, **2**, to **3** (Table 1). It is noticed that compared with $\text{Ir}(\text{pbi})_2\text{acac}$ ($\text{pbi} = 2\text{-phenyl-}N\text{-phenyl benzimidazole}$, $\text{acac} = \text{acetyl acetone}$, $\Phi_{\text{PL}} = 0.73$)⁴² **1** has much lower PL efficiency of only 0.2. The wrapping of the light-emitting cores by optical inertia hexyls should be the main reason for this remarkable decreasing. By the modification with carbazoles, **2** has the double PL efficiency of 0.34. Along with increasing of the density of carbazole moieties Φ_{PL} of **3** greatly increases to 0.72, which is already equal with that of $\text{Ir}(\text{pbi})_2\text{acac}$. It indicates that as the energy-absorbing antennas in the complexes, the peripheral carbazoles can remarkably improve the efficiency of intra- and intermolecular energy transfer. Significantly, from solution to film the PL QY of **1** and **2** remarkably decreased by 45 and 40%, respectively. However, for **3** this reduction of efficiency mainly induced by aggregation variation was only 15%. Obviously, the weakest intermolecular interaction of **3** should be one of the most important reasons for its smallest reduction of PL QY in solid. It is also indicated that increasing the density of carbazole end-

**Figure 5.** CV curves of the ligands.

capped aliphatic chains can realize the simultaneous improvements in sensitizing and separating Ir^{3+} cores. However, the unusually steep increasing of PL QY from **2** to **3** implies that there should be other important factors. It is believed that long lifetime would increase the possibility of the interaction between excited states, so the short lifetime facilitates the reduction of T-T annihilation. The lifetime (τ_{PH}) of these complexes were measured in air at room temperature and listed in Table 1. τ_{PH} of **2** (0.34 μs) is slightly shorter than that of **1** (0.39 μs), but for **3** its lifetime steeply decreases to 0.2 μs , which successfully fits to the trend of their PL QY. Thus with the amorphous state and shortest lifetime **3** exhibits much improved PL efficiencies. With the stable PL emission and PL QY of 0.72 in solution and 0.61 in solid, **3** is favorable among the green-emitting Ir^{3+} complexes. It proves that increasing the density of the surrounding carbazole moieties assuredly improves the optical performance of the complex.

Electrochemical Properties. To demonstrate the contribution of the peripheral carbazole moieties on the carrier injection in the complexes, circle voltammetry (CV) analysis of the ligands and complexes was performed at room temperature in acetonitrile measured against a Ag/Ag^+ electrode (0.34 V vs saturated calomel electrode (SCE)) with tetrabutylammonium hexafluorophosphate (0.1 M in acetonitrile) as the supporting electrolyte (Figures 5 and 6 and Table 1). All of the ligands have similar irreversible reduction peaks attributed to the phenyl benzimidazole moieties. Because of the electron-donating effect of the alkoxy, the reduction potential of Cz_2PhBI is higher than those of other two ligands. According to the equation reported by de Leeuw et al.,⁴³ $E_{\text{HOMO}} = -(E_{\text{onset}}^{\text{Ox}} - \text{SCE} + 4.4 \text{ eV})$ and $E_{\text{LUMO}} = -(E_{\text{onset}}^{\text{Red}} - \text{SCE} + 4.4 \text{ eV})$, all of the ligands have LUMO levels around -3.0 eV, which are comparable with the common electron-transporting materials Alq_3 and TPBI. HexPhBI only has one irreversible oxidation peak with very high potential of 2.25 V, corresponding to HOMO level of -6.39 eV. Thus, HexPhBI has weak hole-injection ability, even hole-blocking ability. For CzPhBI, except for the oxidation peak originated from the PBI moieties, the irreversible oxidation peak at 1.44

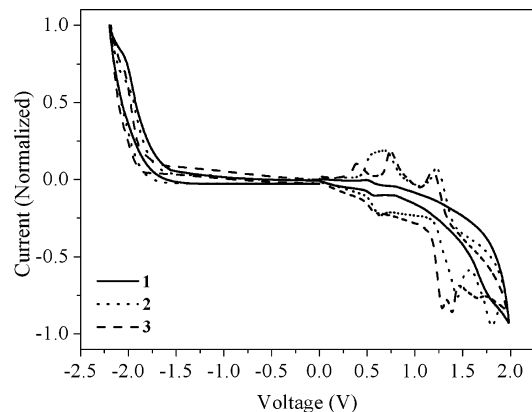


Figure 6. CV curves of **1–3**.

V is attributed to the carbazole moieties. After introducing carbazole moieties HOMO level of CzPhBI rises to -5.92 eV. Cz₂PhBI has a reversible oxidation peak at 1.47 V also attributed to its carbazole moieties. The difference between CzPhBI and Cz₂PhBI is that for Cz₂PhBI there is a distinct shoulder peak at 1.25 V, which means that the carbazole groups in two different environments exhibit different oxidation behaviors. Compared with the oxidation curve of CzPhBI and the Gaussian simulation results in the following section, the shoulder peak should correspond to the carbazole moieties bonded with the phenyls. This results in a further raise of HOMO level of Cz₂PhBI as -5.74 eV.

All of the complexes have irreversible reduction peaks attributed to their benzimidazole moieties, which are similar to those of their ligands. The first reversible oxidation peaks of **1–3** around 0.5 V are originated from Ir³⁺. It was found that for **1** the intensity of its first oxidation peak is much weaker than those of **2** and **3**. The main reason should be that in **1** the Ir³⁺ cores are wrapped by electric inertia hexyls, which restrains the intermolecular carrier transporting. Compared with the ligands, the potentials of the irreversible oxidation peaks attributed to the phenyl moieties of the complexes (around 1.75 V) remarkably decrease, which should be induced by the formation of C–Ir bonds. Because of the electron-donating effect of hexyloxy for **3**, this peak shifts to the lower voltage about 1.6 V. Both of **2** and **3** have the reversible oxidation peaks originated from their carbazoles. Different with **2**, the carbazole moieties bonded with the phenyls and benzimidazoles in **3** revealed two different oxidation peaks, whose potential gap is 110 mV. It is believed that the intramolecular potential gaps facilitate the intramolecular charge transfer, and high intramolecular charge mobility might form the basis of the charge transporting materials.⁴⁴ Thus, its more oxidation states might be anticipated to make **3** superior to **1** and **2** in hole injection and transporting.

Theoretical Calculation. To understand the nature of the electrochemical and optical properties of **1–3**, DFT calculations

were conducted employing the Gaussian 03 package. Different with HexPhBI whose electron clouds of HOMO and LUMO levels are located on the phenyl benzimidazole group, CzPhBI and Cz₂PhBI are donor–acceptor system with flexible hexyls as linker, in which HOMO levels and LUMO levels are contributed by carbazole moieties and phenyl benzimidazole moieties, respectively (Supporting Information S11). Notably, the electron clouds of HOMO and HOMO-1 levels of Cz₂PhBI are located on the two different carbazoles bonding to phenyl and benzimidazole, respectively. This is just in agreement with the oxidation curve of Cz₂PhBI in which the shoulder oxidation peak is attributed to the former carbazole and the main oxidation peak is attributed to the latter. Furthermore, the energy gap between HOMO and HOMO-1 levels of Cz₂PhBI is 27 meV, which is in accord with the potential gap of 22 mV between its oxidation peaks. Obviously, the carbazole bonded with the phenyl makes a remarkable contribution to improve the hole-injection ability of the ligands.

The contour plots of the six lowest unoccupied (LUMO to LUMO+5) and the six highest occupied molecular orbitals (HOMO to HOMO-5) for **1–3** are presented in Supporting Information SI2. As shown in Table 2, HOMO of **1** and **2** involves the contributions of Ir 7d and 8d orbitals (52.4%) and a π orbital localized on the phenyl (ca. 47%). Differently, the oxygen atoms of **3** make an unnegligible contribution of 0.71% to its HOMO, which induce a drop of 1% of the contribution of Ir d orbitals to HOMO of **3**. LUMOs of the complexes are largely dominated by the π^* orbitals of phenyl-benzimidazole moieties with very small contributions of Ir d orbitals. The closed HOMO and LUMO levels of the complexes are in agreement with the electrochemical results. Moreover, the energy gap of **3** is 0.1 eV larger than those of **1** and **2**, which may induce the emission blue shift of about 7 nm. This result is also consistent with the optical analysis results. Furthermore, it is showed that HOMO-3 to HOMO-5 of **2** are attributed to its three carbazole moieties. The electron-cloud densities of HOMO-5 to HOMO-7 of **3** are located on its three carbazole moieties bonded with the phenyls, and its HOMO-8 to HOMO-10 are mainly contributed by the other three carbazole moieties. Although the carbazole moieties in **2** and **3** do not participate in the formation of the HOMO levels, obviously, as the peripheral groups of the cores they are the bridges between different complex molecules and play very important roles in hole-injection/transporting.

EL Properties. Inspired by the amorphous states and excellent PL and electrochemical properties of **2** and **3**, the host-free device **A** and **B** with the configuration of ITO/PEDOT:PSS (50 nm)/Ir³⁺ complexes (40 nm)/TPBI (30 nm)/LiF (1 nm)/Al (100 nm) were fabricated by spin-coat. Device **A** and **B** were based on **2** and **3** respectively. **B** had the much lower turn-on voltage (2.5 V) than that of **A** (3.5 V) (Figure 7). At the same voltages, the current densities (J) of **B** were much bigger than those of **A**. Therefore, through increasing the density of pendant

TABLE 2: The Contribution of d Orbitals of Iridium to the Frontier Orbitals and the Frontier Energy Levels of the Compounds

compound	proportion (%)						HOMO (eV)	LUMO (eV)	E_g (eV)
	HOMO-2	HOMO-1	HOMO	LUMO	LUMO+1	LUMO+2			
HexPhBI							-5.66	-0.93	4.73
CzPhBI							-5.36	-1.01	4.35
Cz ₂ PhBI							-5.33	-0.79	4.54
1	54.86	47.47	52.43	2.09	0.55	2.97	-4.44	-0.82	3.62
2	48.91	47.13	52.45	1.79	0.84	3.02	-4.60	-0.98	3.62
3	45.98	44.99	51.40	1.95	0.07	2.31	-4.54	-0.82	3.72

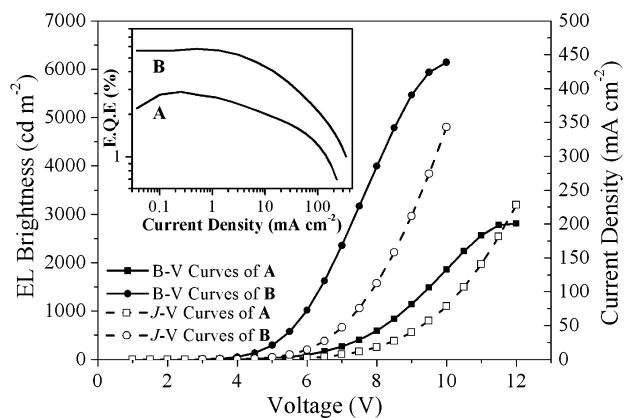


Figure 7. B-V curves and EQE-J curves of the spin-coating host-free device **A** and **B**.

functional groups, the carrier-injection and transport can be efficiently improved, which is in agreement with the electrochemical results. The maximum brightness of **B** was 6150 cd m^{-2} , which was more than twice of that of **A** (2808 cd m^{-2}). Moreover, the ratio of the brightness of **B** and **A** was nearly fixed at the different current densities. It is more inspiring that EQE of **B** at 100 cd m^{-2} was as high as 5.9%, which is equal with that of a device using a blend of 8% (*t*-butyl) phenyl benzimidazole Ir^{3+} complex and 30% PBD in PFO¹⁵ as the emitting layer, higher than those devices based on the green-emitting electrophosphorescent Ir^{3+} polymers^{21,22} and comparable with those of host-free spin-coat devices based on the similar carbazole dendrons substituted phenyl benzimidazole Ir^{3+} complexes.^{27,30} At 1000 cd m^{-2} , the efficiency of **B** remained as 4.5%. It is shown that **B** had much higher efficiencies than **A**, whose EQE were 2.5% at 100 cd m^{-2} and 1.7% at 1000 cd m^{-2} . In addition, the ratios of EQE of **B** to **A** were 2.36, 2.65, and 3.02 at 100, 1000, and 2000 cd m^{-2} , respectively. Since high luminance generally corresponds to high exciton-concentration, it indicates that **3** has much stronger ability to reduce the concentration quenching and T-T annihilation effect than **2**, and at higher exciton concentrations the predominance of **3** became more distinct, which is precisely consistent with our molecular design.

Another question is whether the much better EL performance of **3** is originated from its molecular structure design, which would induce the better carrier injection/transporting, more efficient separation of triplet excitons and weaker intermolecular interaction in **3**, or is attributed to the better luminescent properties of its alkoxy substituted complex core. In order to find out the origin of the highly improved EL performance of **3**, the phosphor-doping devices **C** and **D** with the configuration of ITO/PEDOT:PSS (50 nm)/ Ir^{3+} complexes: TCTA (20%, 40 nm)/TPBI (30 nm)/LiF (1 nm)/Al (100 nm) were also fabricated by spin-coat, corresponding to **2** and **3** respectively. Herein, TCTA was hole-transporting host. The turn-on voltages of **C** and **D** were 3.5 V (Figure 8). **C** had the maximum brightness of 9812 cd m^{-2} at 13 V with current density of 220 mA cm^{-2} . The maximum EQE of **C** reached 11.4% at 5 V with very low current density of 0.22 mA cm^{-2} . The maximum brightness of **D** was 10521 cd m^{-2} at 11 V with current density of 204 mA cm^{-2} . Its maximum efficiency of 9.2% was achieved at 7.5 V with current density of 10.6 mA cm^{-2} . Since at the low voltages the carrier injection/transporting was mainly determined by the host TCTA, **C** and **D** had the same turn-on voltage. However, along with the voltage increasing, at high current density the carrier injection/transporting ability of the guests with the high

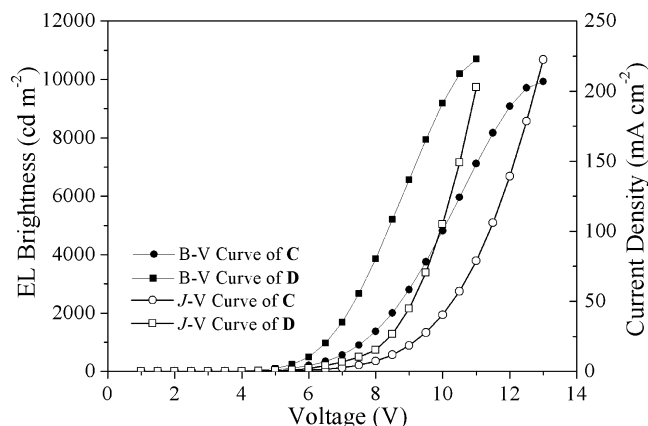


Figure 8. B-V curves of the spin-coating doping device **C** and **D**.

doping concentration of 20% remarkably influenced the carrier injection and transporting in the devices. Compound **3** with the better carrier injection/transporting ability supported the rapid increasing of the current density during the voltage increasing. However, for **2** to obtain the same current density with that of **D** much higher voltage was required. In the doping devices, the host mainly has the strong effect on dispersing light-emitting centers and improving the energy transfer. Thus, for **C** and **D**, TCTA could efficiently restrain the concentration quenching and T-T annihilation. It is noticeable that **C** and **D** had similar maximum brightness and efficiencies, which suggested that the emission cores in **2** and **3** actually have the similar EL properties. Moreover, compared with host-free **A**, both of the brightness and efficiency of phosphor-doping **C** increased 5 times. However, compared with **B** these data of **D** were only improved for 2 and 1.5 times. Obviously, the dispersion ability of TCTA played the crucial role in the performance improvement from **A** to **C**. The remarkable differences between **A** and **B** must be mainly originated from the much stronger encapsulation and improved carrier injection/transporting ability of **3**. Therefore, to achieve a good EL performance at least two-position encapsulation is necessary for the ligand structure design of small-molecular phosphorescent emitters. It is also noticed that although **D** had higher efficiencies at bigger current densities and exhibited stronger efficiency stability, the maximum efficiency of **C** was more than that of **D**. In doping devices, at the much low current densities, the excitons were first formed on the host TCTA. Then the energy transported from the host to the complexes through either the exciton migration or Förster energy transfer, the more thorough encapsulation of the cores in **3** makes TCTA more difficult to get close to the light-emitting cores, which might limit the probability of the exciton migration. The restraining of host-guest energy transfer in **3** due to the higher encapsulation density might be the main reason for its lower maximum efficiencies at low current density. At the high current densities, the stronger encapsulation of the cores and the enhanced carrier injection/transporting ability of **3** supported considerably stable efficiencies and facile carrier-trapping, which made the efficiency of **D** gradually exceed that of **C**.

EL emissions of **A**–**D** were similar with the PL emissions in solid of the corresponding complexes (Figure 9). It is noticeable that compared with **C** the shoulder peaks at 550 nm in the EL spectra of **A** were much stronger. Only at 12 V the intensity of this peak in the spectrum of **C** is comparable with that of **A**. Moreover, the emissions of **A** were slightly wider than those of **C**. Although the shoulder peaks at 520 nm in the spectra of **B** were also enhanced during the voltage increasing, the spectra of **B** and **D** were almost the same at the same

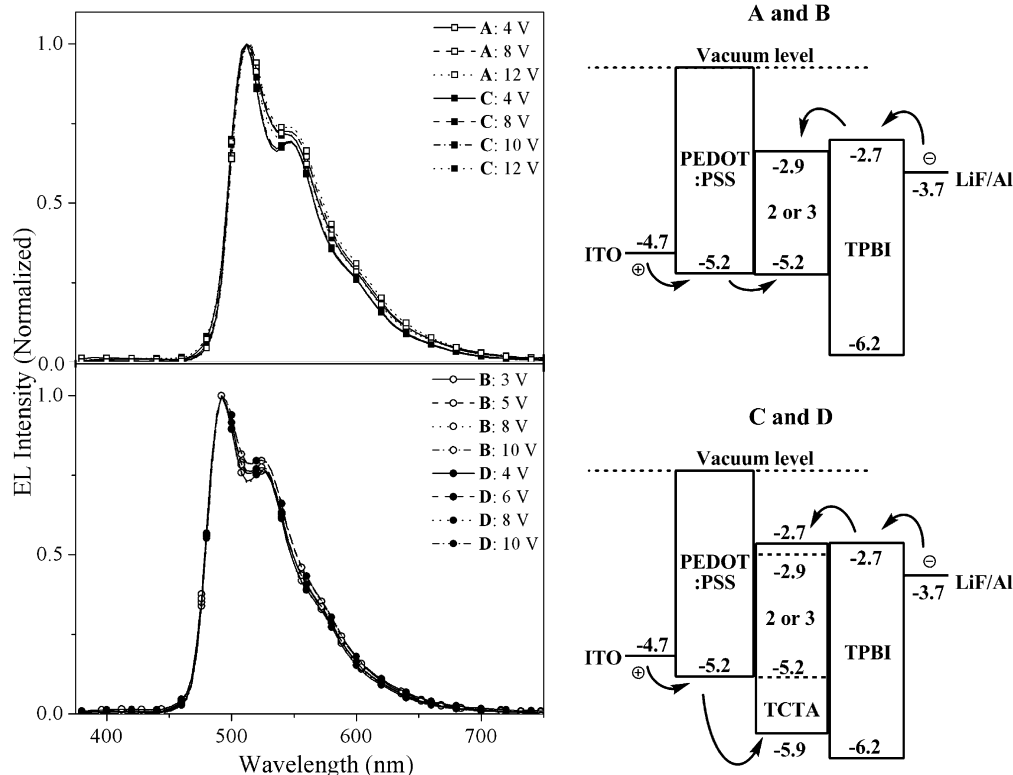


Figure 9. EL spectra of A–D at different voltages and schemes of energy levels of A–D.

voltages. The enhancement of the shoulder peak might be induced by the intermolecular interaction at high exciton concentrations. Even at the lower exciton concentrations, **2** exhibited considerably strong interaction, which might be the reason for the differences between the emissions of A and C. However, **3** only exhibited relatively strong interaction at much higher exciton concentrations. The same EL spectra of B and D also indicated the weakened intermolecular interaction in **3**.

Conclusion

In this work, we have synthesized a simple phenyl benzimidazole Ir³⁺ complex **3** with the six-arm encapsulation. Our investigation showed that the combined modification of the aliphatic chains and functional groups in multipositions is a feasible approach to realize the high-efficiency small molecular phosphorescent materials in which the wrapping effect of the aliphatic chains and the encapsulation effect of the functional groups are utilized to reduce the concentration quenching and T-T annihilation effect. Compounds **3** and **2** end-capped with the conjugated carbazole moieties have improved thermal stability than the hexyl-substituted **1**. XRD analysis proved that the carbazole end-capped aliphatic groups have stronger effect on restrain the aggregation. Both **2** and **3** are amorphous. Compound **3** exhibits much better PL properties in solution and solid than **1** and **2**. The peripheral carbazoles not only facilitate the separation of triplet-emission cores, but also supply a routine for the intermolecular energy transfer. Significantly, for **3** the reduction of PL efficiency from solution to solid mainly induced by aggregation variation was only 15%, which is only a half of those of **1** and **2**. Both electrochemical analysis and Gaussian simulation suggested the important role of the peripheral carbazoles in carrier injection/transporting. Furthermore, the more oxidation states of **3** might be anticipated to make it superior to **1** and **2** in hole injection and transporting. A dramatic EQE of nearly 6% from the host-free spin-coated device of **3**

was achieved. The device also had very low turn-on voltage of 2.5 V and high brightness over 6000 cd m⁻². Compared with **2**, **3** exhibited much better EL performances, such as bigger brightness and higher efficiency, which are mainly attributed to its reduced intermolecular interaction, improved carrier injection/transporting ability, and limited emission quenching.

Acknowledgment. This work was financially supported by NSFC under Grants 50903028 and 20972043, Natural Science Foundation of Heilongjiang province under Grant QC08C10, Education Bureau of Heilongjiang Province under Grants 11521206 and 11521216, Key Laboratory of Optical Electronics and Energy/Environmental Materials of Heilongjiang Province, and Heilongjiang University Starting Foundation of Young Teachers. The authors want to thank Dr. Qiang Li, Dr. Chun-Gui Tian, and Dr. Ju-Wen Zhang for their assistance in the thermal, XRD, and electrochemical analysis.

Supporting Information Available: The contours of frontier molecular orbitals of the ligands and complexes simulated with Gaussian 03. This material is available free of charge via the Internet at <http://pubs.acs.org>.

References and Notes

- (1) Baldo, M. A.; O'Brien, D. F.; You, Y.; Shoustikov, A.; Sibley, S.; Thompson, M. E.; Forrest, S. R. *Nature* **1998**, *395*, 151.
- (2) Baldo, M. A.; Lamansky, S.; Burrows, P. E.; Thompson, M. E.; Forrest, S. R. *Appl. Phys. Lett.* **1999**, *75*, 4.
- (3) Forrest, S. R. *Nature* **2004**, *428*, 911.
- (4) Tsutsui, T.; Yang, M. J.; Yahiro, M.; Nakamura, K.; Watanabe, T.; Tsuji, T.; Fukuda, Y.; Wakimoto, T.; Miyaguchi, S. *Jpn. J. Appl. Phys., Part 2* **1999**, *38*, L1502.
- (5) Adachi, C.; Baldo, M. A.; Thompson, M. E.; Forrest, S. R. *J. Appl. Phys.* **2001**, *90*, 5048.
- (6) Holmes, R. J.; D'Andrade, B. W.; Forrest, S. R.; Ren, X.; Li, J.; Thompson, M. E. *Appl. Phys. Lett.* **2003**, *83*, 3818.
- (7) Yeh, S. J.; Wu, M. F.; Chen, C. T.; Song, Y. H.; Chi, Y.; Ho, M. H.; Hsu, S. F.; Chen, C. H. *Adv. Mater.* **2005**, *17*, 285.

- (8) Yang, M. J.; Tsutsui, T. *Jpn. J. Appl. Phys., Part 2* **2000**, *39*, L828.
- (9) Gong, X.; Robinson, M. R.; Ostrowski, J. C.; Moses, D.; Bazan, G. C.; Heeger, A. J. *Adv. Mater.* **2002**, *14*, 581.
- (10) Takizawa, S.; Montes, V. A.; Anzenbacher, P., Jr. *Chem. Mater.* **2009**, *21*, 2452.
- (11) Tao, Y. T.; Wang, Q.; Yang, C. L.; Zhang, K.; Wang, Q.; Zou, T. T.; Qin, J. G.; Ma, D. G. *J. Mater. Chem.* **2008**, *18*, 4091.
- (12) Zhang, K.; Chen, Z.; Yang, C. L.; Zhang, X. W.; Tao, Y. T.; Duan, L.; Chen, L.; Zhu, L. N.; Qin, J. G.; Cao, Y. *J. Mater. Chem.* **2007**, *17*, 3451.
- (13) Tao, Y. T.; Wang, Q.; Yang, C. L.; Wang, Q.; Zhang, Z. Q.; Zou, T. T.; Qin, J. G.; Ma, D. G. *Angew. Chem., Int. Ed.* **2008**, *47*, 8104.
- (14) Shen, F.-Z.; Xia, H.; Zhang, C.-B.; Lin, D.; He, L.; Ma, Y. G. *J. Phys. Chem. B* **2004**, *108*, 1014–1019.
- (15) Wei, X. Q.; Peng, J. B.; Cheng, J. B.; Xie, M. G.; Lu, Z. Y.; Li, C.; Cao, Y. *Adv. Funct. Mater.* **2007**, *17*, 3319.
- (16) Mi, B. X.; Wang, P. F.; Gao, Z. Q.; Lee, C. S.; Lee, S. T.; Hong, H. L.; Chen, X. M.; Wong, M. S.; Xia, P. F.; Cheah, K. W.; Chen, C. H.; Huang, W. *Adv. Mater.* **2008**, *20*, 1.
- (17) Xiao, L. X.; Su, S.-J.; Agata, Y.; Lan, H.; Kido, J. *Adv. Mater.* **2009**, *21*, 1271.
- (18) Chen, X.; Liao, J.-L.; Liang, Y.; Ahmed, M. O.; Tseng, H.-E.; Chen, S.-A. *J. Am. Chem. Soc.* **2003**, *125*, 636.
- (19) Sandee, A. J.; Williams, C. K.; Evans, N. R.; Davies, J. E.; Boothby, C. E.; Köhler, A.; Friend, R. H.; Holmes, A. B. *J. Am. Chem. Soc.* **2004**, *126*, 7041.
- (20) Liu, S.-J.; Zhao, Q.; Deng, Y.; Xia, Y.-J.; Lin, J.; Fan, Q.-L.; Wang, L.-H.; Huang, W. *J. Phys. Chem. C* **2007**, *111*, 1166.
- (21) Zhen, H. Y.; Luo, J.; Yang, W.; Chen, Q. L.; Ying, L.; Zou, J. H.; Wu, H. B.; Cao, Y. *J. Mater. Chem.* **2007**, *17*, 2824.
- (22) Zhen, H. Y.; Jiang, C. Y.; Yang, W.; Jiang, J. X.; Huang, F.; Cao, Y. *Chem.—Eur. J.* **2005**, *11*, 5007.
- (23) Halim, M.; Pillow, J. N. G.; Samuel, I. D. W.; Burn, P. L. *Adv. Mater.* **1999**, *11*, 371.
- (24) Freeman, A. W.; Koene, S. C.; Malenfant, P. R. L.; Thompson, M. E.; Frechet, J. M. J. *J. Am. Chem. Soc.* **2000**, *122*, 12385.
- (25) Lo, S. C.; Anthopoulos, T. D.; Nanddas, E. B.; Burn, P. L.; Samuel, I. D. W. *Adv. Mater.* **2005**, *17*, 1945.
- (26) Bolink, H. J.; Santamaria, S. G.; Sudhakar, S.; Zhen, C. G.; Sellinger, A. *Chem. Commun.* **2008**, 618.
- (27) Burn, P. L.; Lo, S.-C.; Samuel, I. D. W. *Adv. Mater.* **2007**, *19*, 1675.
- (28) Zhang, K.; Chen, Z.; Zou, Y.; Gong, S. L.; Yang, C. L.; Qin, J. G.; Cao, Y. *Chem. Mater.* **2009**, *21*, 3306.
- (29) (a) Zhou, G. J.; Wong, W.-Y.; Yao, B.; Xie, Z. Y.; Wang, L. X. *Angew. Chem., Int. Ed.* **2007**, *46*, 1149. (b) Zhou, G. J.; Wong, W.-Y.; Yao, B.; Xie, Z. Y.; Wang, L. X. *Angew. Chem.* **2007**, *119*, 1167.
- (30) Ding, J. Q.; Gao, J.; Cheng, Y. X.; Xie, Z. Y.; Wang, L. X.; Ma, D. G.; Jing, X. B.; Wang, F. S. *Adv. Funct. Mater.* **2006**, *16*, 575.
- (31) Wang, Y.; Herron, N.; Grushin, V. V.; LeCloux, D.; Petrov, V. *Appl. Phys. Lett.* **2001**, *79*, 449.
- (32) Song, Y. H.; Yeh, S. J.; Chen, C. T.; Chi, Y.; Liu, C. S.; Yu, J. K.; Hu, Y. H.; Chou, P. T.; Peng, S. M.; Lee, G. H. *Adv. Funct. Mater.* **2004**, *14*, 1221.
- (33) Lowry, M. S.; Goldsmith, J. I.; Slinker, J. D.; Rohl, R.; Pascal, R. A., Jr.; Malliaras, G. G.; Bernhard, S. *Chem. Mater.* **2005**, *17*, 5712.
- (34) Liu, Z. W.; Guan, M.; Bian, Z. Q.; Nie, D. B.; Gong, Z. L.; Li, Z. B.; Huang, C. H. *Adv. Funct. Mater.* **2006**, *16*, 1441.
- (35) Liu, Y.; Ye, K. Q.; Fan, Y.; Song, W. F.; Wang, Y.; Hou, Z. M. *Chem. Commun.* **2009**, 3699.
- (36) Xu, H.; Xu, Z.-F.; Yue, Z.-Y.; Yan, P.-F.; Wang, B.; Jia, L.-W.; Li, G.-M.; Sun, W.-B.; Zhang, J.-W. *J. Phys. Chem. C* **2008**, *112*, 15517.
- (37) Becke, A. D. *J. Chem. Phys.* **1993**, *98*, 5648–5652. (b) Lee, C.; Yang, W.; Parr, R. G. *Phys. Rev. B* **1988**, *37*, 785–789.
- (38) Hay, P. J. *J. Phys. Chem. A* **2002**, *106*, 1634–1641.
- (39) Frisch, M. J.; Trucks, G. W.; Schlegel, H. B.; Scuseria, G. E.; Robb, M. A.; Cheeseman, J. R.; Montgomery, J. A., Jr.; Vreynen, T.; Kudin, K. N.; Burant, J. C.; Millam, J. M.; Iyengar, S. S.; Tomasi, J.; Barone, V.; Mennucci, B.; Cossi, M.; Scalmani, G.; Rega, N.; Petersson, G. A.; Nakatsuji, H.; Hada, M.; Ehara, M.; Toyota, K.; Fukuda, R.; Hasegawa, J.; Ishida, M.; Nakajima, T.; Honda, Y.; Kitao, O.; Nakai, H.; Klene, M.; Li, X.; Knox, J. E.; Hratchian, H. P.; Cross, J. B.; Adamo, C.; Jaramillo, J.; Gomperts, R.; Stratmann, R. E.; Yazyev, O.; Austin, A. J.; Cammi, R.; Pomelli, C.; Ochterski, J. W.; Ayala, P. Y.; Morokuma, K.; Voth, G. A.; Salvador, P.; Dannenberg, J. J.; Zakrzewski, V. G.; Dapprich, S.; Daniels, A. D.; Strain, M. C.; Farkas, O.; Malick, D. K.; Rabuck, A. D.; Raghavachari, K.; Foresman, J. B.; Ortiz, J. V.; Cui, Q.; Baboul, A. G.; Clifford, S.; Cioslowski, J.; Stefanov, B. B.; Liu, G.; Liashenko, A.; Piskorz, P.; Komaromi, I.; L. Martin, R.; Fox, D. J.; Keith, T.; Al-Laham, M. A.; Peng, C. Y.; Nanayakkara, A.; Challacombe, M.; Gill, P. M. W.; Johnson, B.; Chen, W.; Wong, M. W.; Gonzalez, C.; Pople, J. A. *Gaussian 03*, rev. C.02; Gaussian, Inc.: Pittsburgh, PA, 2004.
- (40) Tamayo, A. B.; Alleyne, B. D.; Djurovich, P. I.; Lamansky, S.; Tsyba, I.; Ho, N. N.; Bau, R.; Thompson, M. E. *J. Am. Chem. Soc.* **2003**, *125*, 7377.
- (41) Gambino, S.; Stevenson, S. G.; Knights, K. A.; Burn, P. L.; Samuel, I. D. W. *Adv. Funct. Mater.* **2009**, *19*, 317.
- (42) Huang, W.-S.; Lin, J. T.; Chien, C.-H.; Tao, Y.-T.; Sun, S.-S.; Wen, Y.-S. *Chem. Mater.* **2004**, *16*, 2480.
- (43) de Leeuw, D. M.; Simenon, M. M. J.; Brown, A. R.; Einerhand, R. E. F. *Synth. Met.* **1997**, *87*, 53.
- (44) Plater, M. J.; Jackson, T. *Tetrahedron* **2003**, *59*, 4673.